Journal of Materials Chemistry B

Accepted Manuscript

ROYAL SOCIETY OF CHEMISTRY

www.rsc.org/materialsB

Journal of Materials Chemistry B

ARTICLE

Porous and strong three-dimensional carbon nanotube coated ceramic scaffolds for tissue engineering

Received 00th January 20xx,
Accepted 00th January 20xx

DOI: 10.1039/x0xx00000x

www.rsc.org/

P. Newman,[a,b] Z. Lu,[a] S. Roohani-Esfahani,[a] T.L. Church,[b,c] M. Biro,[d,e] B. Davies,[a,b] A. King,[b] K. Mackenzie,[b] A.I. Minett[b] and H. Zreiqat[a]

Biomaterials research is investigating increasingly complex materials capable of mirroring the highly organized biochemical and architectural environments of the body. Accordingly, tissue scaffolds with nanoscale properties that mirror the fibrous proteins present in tissue are being developed. Such materials can benefit from the inherent dimensional similarities and nanocomposite nature of the cellular environment, altering nanoscale dimensional and biochemical properties to mimic the regulatory characteristics of natural cellular environments. One nanomaterial which demonstrates potential across a diverse range of biomaterial applications is carbon nanotubes (CNTs). Building on previous reports, a method to coat CNTs throughout 3D porous structures is developed. Through modifications to typical chemical vapour deposition (CVD), a high-quality uniform coating of carbon nanotubes (CNTs) is demonstrated over β-tricalcium phosphate/hydroxyaptite (or TCP/HA), which is in clinical use; and the high-mechanical-strength multicomponent ceramic $Ca_2ZnSi_2O_7$-$ZnAl_2O_4$, (or Sr-HT-Gah). The resulting materials address deficiencies of previously reported CNT biomaterials by simultaneously presenting properties of high porosity, biocompatibility and a mechanical stability. Together, this unique combination of properties makes these scaffolds versatile materials for tissue engineering in load bearing applications.

Introduction

Tissue engineering focuses on the development of materials to regenerate damaged tissue and organs. These materials mirror the structure and functions of the cellular environment to facilitate cell growth and help restore tissue function. One approach uses nanomaterials which can mimic the nanoscale dimensional properties of the fibrous protein polymers present in tissue. Such nanomaterials show promise for use as biomaterial scaffolds and have shown nanoscale dimensionality to be an effective regulator of cell behavior in the absence of more traditional biochemical regulators, such as cytokines or growth factors.[1,2] This potential is further extended by the extraordinary material properties of nanomaterials, which can be leveraged when used alone or as composite materials.

One class of nanomaterial with potential in such applications is carbon nanotubes (CNTs). Leveraging the extraordinary properties of these versatile graphitic tubes, materials scientists have demonstrated a diverse range of applications including high strength composites[3] and woven fibers[4] as well as high performance batteries, capacitors,[5] sensors and actuators.[6,7] This diversity also extends to healthcare applications including drug and gene delivery, pathogen and biosensing, cancer therapies, bio-imaging and tissue engineering.[8,9] For tissue engineering applications, CNTs have demonstrated potential for the regeneration across a range of tissue types including bone,[10-12] cartilage,[13] muscle,[14,15] and nerve tissue.[16-18]

Despite the demonstrated potential for CNTs in a diverse range of biomaterial applications, their implementation remains problematic. For practical reasons, a number of reports have assessed the feasibility of CNT biomaterials using 2D film substrates.[19-27] Such film materials lack the dimensionality and porosity required to be successful in many tissue engineering applications, as they do not replicate tissue structure or allow vascularization and transport of nutrients and waste. Similarly, although three-dimensional CNT materials have been reported for tissue engineering applications,[11,28-34] they have yet to meet the combined properties necessary for tissue regeneration in a 3D environment. They have to date either lacked sufficient porosity (necessary for applications requiring cellular ingrowth and vascularization)[28-31] or toughness (for applications with demanding mechanical requirements),[28-34] or have been composite materials.[11,32,33] For such composites the interaction with CNTs is confined to points at which they are coincident to the composites surface. Further, in such cases,

[a] Biomaterials and Tissue Engineering Research Unit, School of Aeronautical Mechanical and Mechatronics Engineering, The University of Sydney, Sydney NSW Australia 2006
[b] Laboratory for Sustainable Technology, School of Chemical and Biomolecular Engineering, The University of Sydney, Sydney NSW Australia 2006
[c] Department of Materials and Environmental Chemistry, Stockholm University, Stockholm, Sweden
[d] Centenary Institute for Cancer Medicine and Cell Biology, Newtown, Sydney NSW Australia 2042
[e] Sydney Medical School, The University of Sydney, Sydney NSW Australia 2006.
E-mail: p.newman@sydney.edu.au, hala.zreiqat@sydney.edu.au

interaction with CNT is confined to low volume percentages (typically 1-5%) of CNT filler within a composite matrix as higher inclusions significantly diminish the mechanical properties of the resulting composite.[3]

The challenge remains to create a 3D CNT material that simultaneously presents properties of high porosity, biocompatibility and mechanical stability. In the present study, we report the fabrication of CNT-coated porous ceramic scaffolds that is biocompatible, highly porous, interconnected and mechanically strong. This was achieved with high quality uniform coatings of CNTs over two different types of 3D porous ceramic scaffolds: the bioceramic composite β-tricalcium phosphate/hydroxyaptite (or TCP/HA); and the mechanically strong multicomponent ceramic ($Ca_2ZnSi_2O_7$-$ZnAl_2O_4$), (or Sr-HT-Gah) developed by our group.[35,36] We show the biocompatability of these CNT-caoted scaffolds showing comparble cell attachment and equivalent cell proliferation relative to the clinically used TCP/HA bioceramic. Additionally, we demonstrate that coating the 3D scaffolds with CNTs does not compromise physical properties including porosity, interconnectivity and mechanical strength.

Experimental Section

Preparation of Porous Ceramic Scaffolds

Porous ceramic scaffolds of TCP/HA and Sr-HT-Gah were prepared as described in [36] and [35], respectively. Briefly, TCP/HA ceramics were fabricated by aqueous precipitation of $Ca(NO_3)_2{\cdot}4H_2O$ (0.92 M) and $(NH_4)_2HPO_4$ (0.58 M) solutions at room temperature and pH 11. This created a biphasic calcium phosphate consisting ~40% HA and 60% β-TCP. To homogenize particle size, powders were ground via ball milling (Retsch Planetary Ball Mill PM 200) for 2 h at 150 rpm. Sr-HT-Gah ceramics were fabricated by first synthesizing Sr–$Ca_2ZnSi_2O_7$ powders via a sol–gel reaction using tetraethyl orthosilicate ($(C_2H_5O)_4Si$, TEOS), zinc nitrate hexahydrate ($Zn(NO_3)_2{\cdot}6H_2O$), calcium nitrate tetrahydrate ($Ca(NO_3)_2{\cdot}4H_2O$) and strontium nitrate ($Sr(NO_3)_2$) as raw materials (all sourced from Sigma–Aldrich, USA). Aluminum oxide (15 wt.%) was introduced to the Sr–$Ca_2ZnSi_2O_7$ powder and ball milled as above. A polyurethane foam sponge replication technique was used to fabricate scaffolds. Fully reticulated polyurethane foam was cut to a cylinder with a diameter of 8 mm and a height of 10 mm, washed with ethanol, and used as a sacrificial template. The ceramic powder was coated over the template in a slurry of ceramic powder (~30 wt%) and polyvinyl alcohol (0.01 M in H_2O). After air drying for 24 h, the coated sponges were fired in an electric furnace using a four-step process. For the TCP/HA scaffolds the process was: i) heating at 1 °C min^{-1} to 600 °C, (ii) heating at 2 °C min^{-1} from 600 °C to 1250 °C, (iii) dwelling at 1250 °C for 2 h and (iv) cooling at 5 °C min^{-1} to 25 °C. For the Sr-HT-Gah scaffolds, this process was identical apart from steps ii) and iii) where the maximum/dwelling temperature was increased to 1270 °C. Following firing, the scaffold dimensions had reduced to a diameter of 6 mm and a height of 8 mm.

Growth of VACNT Arrays over Porous Ceramics

Ceramic scaffolds of TCP/HA or Sr-HT-Gah were coated with vertically aligned carbon nanotubes (VACNTs) using CVD in a dual-zone furnace (OTF-1200 × 2-II, MTI) containing a cylindrical quartz tube (inside diameter 44 mm, length 700 mm). Gas flows (Ar, H_2, C_2H_4, and CO_2) were controlled using Alicat Scientific mass-flow controllers. The CNT catalyst precursor Ferrocene (Fc) (100 mg, ≥98%, Sigma-Aldrich) was placed in an alumina crucible in the first zone, while the ceramic scaffolds were placed in the second zone atop an alumina platform that suspended the scaffolds at the center point of the circular cross-section of the quartz tube. The CNT growth process was performed in two phases: an initial catalyst-deposition phase followed by the CNT growth phase. During catalyst deposition, the first zone was heated to 250 °C over 75 min under 0.0165 L min^{-1} Ar (for optimal synthesis conditions) to sublime Fc. Concurrently the second zone was heated to 770 °C (for TCP/HA scaffolds) or 745 °C (for Sr-HT-Gah scaffolds) over 75 min, causing the Fc vapor to decompose and form the Fe nanoparticles over the scaffolds that catalyze CNT growth. The low flow rate used minimized turbulence, the chaotic nature of which precluded the even distribution of CNT catalysts precursors in other experiments using higher flow rates. Using lower flow, or no gas flow, during catalyst deposition resulted in a backflow of gases and Fc recrystallization rather than decomposition over the scaffolds. Following catalyst deposition, the temperature was then maintained at 250 and 750 °C in the first and second zones, respectively, while 0.25 L/min $H_2/Ar/C_2H_4$ in the ratios 6/17/5 respectively as well as 4500 ppm CO_2 flowed through the tube. After 5 min, the furnace was cooled to ambient temperature under a flow of 0.5 L min^{-1} Ar.

Ultrastructural Characterization of CNT Scaffolds

Scaffolds were cut in half along their height/long axis using a surgical scalpel to expose a rectangular cross-section where the interface between the ceramic and CNT coating could be observed. The morphology of the CNT coatings was then observed using field-emission scanning electron microscopy (FESEM, Zeiss Ultra plus). The CNT diameters were analyzed from measurements of 884 nanotubes using high-resolution transmission electron microscopy (HRTEM, Philips CM120 Biofilter). Scaffolds were crushed with a mortar and pestle, mixed with 20 mL of ethanol, and bath sonicated for 15 min before three drops of the resulting mixture were pipetted onto a 200 mesh copper grid (coated with lacey carbon film) and air dried.

CNT quality was assessed using Raman spectroscopy performed at room temperature using a Renishaw Raman with 10 mW Ar^+ laser (filtered to 10% power) at 514 nm excitation fitted through a compound microscope with x20 objective and 5 sec acquisition time. Low laser power and acquisition time ensure minimal deviation from ambient conditions which could affect the Raman spectra of the CNTs.[37, 38]

Measurement of Scaffold Surface Area and Porosity

The surface area and interparticle porosity of the scaffolds and composites were determined from N_2 adsorption–desorption isotherms measured at 77 K on a Quantachrome iQ sorption instrument. Samples were monoliths and were degassed at 150 ºC for 12 h before measurement. The Brunauer–Emmett–Teller surface areas[39] were calculated from the portion of the isotherm with P/P_o = 0.05–0.25, and pore-size distributions were calculated according to the Barrett–Joyner–Halenda method[40] using data from the adsorption branch.

The three-dimensional architecture of the porous scaffolds was assessed by microcomputed X-ray tomography (μCT; SkyScan 1072, Belgium). Porosity was determined in Image J by importing image stacks and averaging the measured scaffold area of each slice/scan with Otsu thresholding. Rendered volume reconstructions were completed with a volume-viewer plugin and were used to measure scaffold pores and determine pore size (n > 60 for each scaffold type).

Ion release from Scaffolds

The leaching of metal ions Fe and Ca from TCP/HA scaffolds was analyzed using inductively coupled plasma–optical emission spectrometry (ICP-AES, Vista AX, Varian). Scaffolds were left in 2 mL of x1 phosphate-buffered saline. At specified time points, 1-mL samples were taken and replaced with 1 mL of fresh saline. This was completed with eight samples each of both CNT-coated and non-coated samples of TCP/HA and Sr-HT-Gah. Samples were diluted 1:20 in 2 wt% HNO3(aq) prior to measurement.

Calibration curves were prepared from 3–5 manually diluted samples prepared from a commercial multi-element standard (CHOICE Analytical) in 4.5 wt% HNO3(aq). All calibration curves were linear with R2 ≥ 0.9799. The spectral lines analyzed were: Ca, 396.847 nm; Fe, 238.204 nm; K, 766.491 nm; Mg, 279.553 nm; and Na, 589.592 nm.

Metal concentrations were averaged over the samples at each given time point. These values were then used to calculate the Fe and Ca released between time points, which can be calculated as the mass of metal measured at a given time point minus the mass of metal that was present after the previous time point, i.e. after the solution had been sampled and replenished with fresh media:

$$(m_{released,i} = m_{measured,i} - m_{measured,(i-1)}/2) \quad (1)$$

The total mass of metal released at time point N can then be calculated by summing the metal released between time points (Eq.1) from i = 1 to i = N:

$$(m_{released,i} = \sum_{i=1}^{N} m_{released,i}) \quad (2)$$

Compressive Strength Measurement

The mechanical properties of eight identical specimens of each sample group (TCP/HA, CNT-TCP/HA, Sr-HT-Gah, CNT-Sr-HT-Gah) were measured. Compressive strength was determined according to ASTM C1424 by crushing cylindrical scaffolds between two flat plates using a computer-controlled universal testing machine (Instron 8874, UK) moving at 0.5 mm min^{-1}.

In Vitro Evaluation by Cell Culture

Permission to use discarded human tissue was granted by the Human Ethics Committee of the University of Sydney and informed consent was obtained. Human trabecular bone was chopped into 1-mm^3 pieces and washed three times in phosphate buffered saline (PBS), followed by digestion in PBS with 0.02% (w/v) trypsin (Sigma–Aldrich) for 90 min at 37 °C. Digested cells were cultured in complete media containing α-Minimal Essential Medium (α-MEM, Gibco Laboratories, Mulgrave, Victoria, Australia), supplemented with 10% (v/v) heat-inactivated fetal calf serum (FCS, Gibco), 2 mM L-glutamine (Gibco), 25 mM Hepes Buffer (Gibco), 2 mM sodium pyruvate, 100 units mL^{-1} penicillin, 100 μg mL^{-1} streptomycin (Gibco) and 1 mM L-ascorbic acid phosphate magnesium salt (Wako Pure Chemicals, Osaka, Japan). The obtained cells, primary human osteoblasts (HOBs), were cultured at 37 °C with 5% CO_2, and the medium was refreshed every 3 d until confluence when cells were passaged. All HOBs used in the experiments were at passage three.

Adipose-derived stem cells (ASCs purchased from Invitrogen, Carlsbad, California) were propagated according to the manufacturer's instructions, and MesenPRO RS Basal Medium with the supplementations of 2 mM L-glutamine and MesenPRO RS Growth Supplement were used. ASCs at passage four were used for the study.

To culture HOBs or ASCs on the scaffolds, a suspension of 100 μL culture medium containing 200,000 cells was dropped gently onto the scaffolds (n = 4) and incubated for 90 min under standard culture conditions to allow the cells to attach to the scaffolds before flooding with the cell culture medium. Before cell seeding, all scaffolds were sterilized by autoclaving at 120 °C for 1 h, then moving to tissue culture plates and soaking in 70% ethanol overnight. Immediately prior to culture, ethanol was aspirated from the scaffolds using a vacuum pump, and they were then rinsed three times with sterilized phosphate-buffered saline (PBS).

Cell attachment was observed using field emission scanning electron microscope (FESEM) (Zeiss Ultra Plus, Germany; secondary electron detector) following cell fixation and dehydration. At 24 h, ASCs were washed twice with PBS, fixed in 4% aqueous paraformaldehyde, post-fixed in osmium tetraoxide and dehydrated with sequential graded ethanol washes. Scaffolds were then dried in hexamethyldisilizane and sputter-coated with gold.

Cell proliferation was determined at 3 and 7 d using a CyQUANT cell proliferation assay including CyQUANT GR dye and cell lysis buffer (Molecular Probes, Australia). Briefly, at the designated time point, culture medium was aspirated from wells and cells were frozen at – 80 ˚C. At a later time, cells were thawed and lysis buffer was added and pipetted through the scaffolds several times before the cell lysate was removed. DNA-binding fluorescent dye was then added to the cell lysates and excited at 497 nm. Emission was measured at 520 nm.[41]

Statistical Analysis

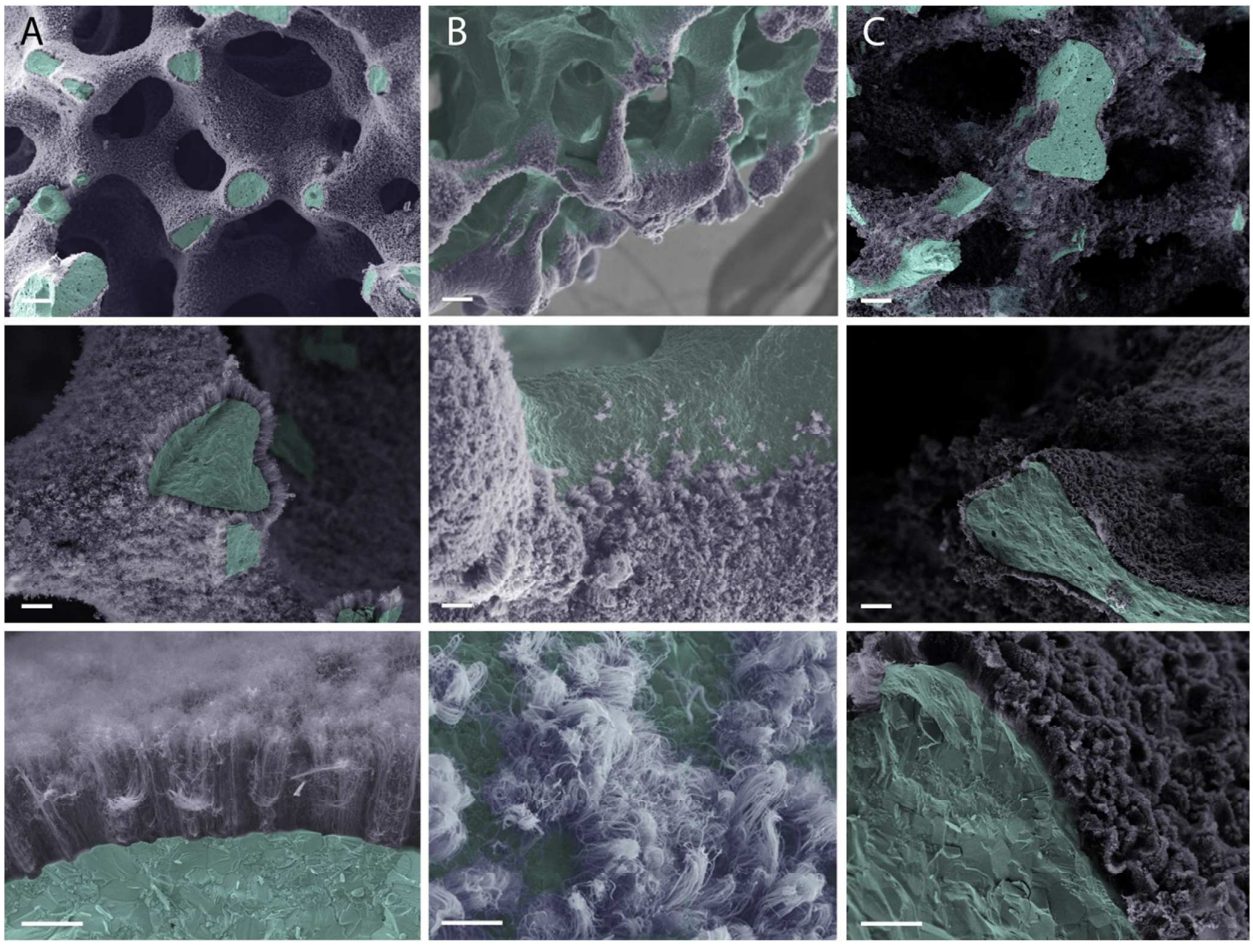

Figure 1. Scanning electron micrographs with false-coloring showing cross-sections of porous Sr-HT-Gah ceramic scaffolds coated with CNTs. CNTs and ceramics are colored purple and teal, respectively. Ceramic can be seen in all images as the scaffolds were cross-sectioned for imaging. Column A shows composites produced under optimized synthesis conditions; here, CNTs infiltrate the entirety of the scaffold without carbonaceous impurities or exposure of the underlying scaffold. Columns B and C show composites generated under sub-optimal synthesis conditions, using either high flow rates during catalyst deposition phase (column B) or performing CNT growth without both CO_2 and higher proportions of H_2 present during CNT growth (column C). Magnification increases downwards, with scale bars in rows 1, 2, 3 corresponding to 100, 10 and 2 µm respectively.

Statistical analysis to determine if the data sets of CNT-coated and uncoated samples were significantly different for compressive strength, cell proliferation and concentration of ions leeched, used an unpaired two-sample Student's t-test. Here, the null hypothesis that the data sets came from independent random samples with normal distributions, equal means and an unknown variance was ascertained at the 5% significance level.

Results and Discussion

Scaffold Fabrication

Nanomaterials display unique size-dependent properties that are not available to the same material at larger scales.[42] As a result, tight control over size and morphology are critical to any nanotechnological application. Reproducibly obtaining homogeneous nanomaterials with a specified property remains among the main challenges of nanoscience. In this work, we optimized CNT synthesis for coating porous ceramic scaffolds. Through alteration to typical CVD synthesis techniques we were able to achieve high-quality uniform coatings of CNTs throughout large (6 mm diameter × 8 mm) porous scaffolds of TCP/HA and Sr-HT-Gah. Sr-HT-Gah was the material of choice as it is 100 times stronger than TCP/HA at the same porosity and interconnectivity. Figure 1 shows scanning electron micrographs of CNT-coated ceramic scaffolds with false coloring. The scaffolds have been cross-sectioned to demonstrate that the synthesis procedure has been optimized to uniformly coat the interior structure of the porous scaffolds. A similar cross-section, reconstructed from micro-CT scans, is shown in Figure 2A. Under optimized conditions, a coating of high-quality CNTs (see Figure 2 and discussion below) of uniform depth, without carbonaceous impurities or bare spots, was produced (Figure 1 Column A). The ceramic interior of the materials produced under these conditions was only visible at points of cross-sectioning. Higher-magnification images of the material produced under optimized conditions (Figure 1A, Row 3) revealed the structure of the coating, which consisted of vertically aligned CNTs

(VACNTs). CNTs align vertically when the formation of adjacent nanotubes prevents growth in directions other than orthogonal to the supporting scaffold, and therefore this alignment indicates that the CNT-growth catalyst was deposited on the underlying ceramic as evenly spaced particles having a narrow size distribution.[43]

Figure 1, Column B shows the CNT-coated Sr-HT-Gah ceramic formed under sub-optimal synthesis conditions, in this case using gas-flow rates typically chosen for CNT growth by CVD.[44] Here, a flow rate of 0.132 L/min Ar was used during the catalyst-deposition phase, resulting in only the exterior of the scaffolds being coated (see Figure 1B, Rows 1 and 2), indicating that the CNT-growth catalyst was only deposited on these surfaces.

Figure 1, Column C shows another CNT-coated Sr-HT-Gah ceramic produced under sub-optimal synthesis conditions. In this case, the gas flow rate (0.25 L/min H_2/Ar/C_2H_4 in the ratios 2/20/5 respectively) was equivalent to the total flow under optimized conditions, but without CO_2 or higher concentrations of H_2 during the CNT-growth phase. This demonstrates the importance of including CO_2 and increased concentrations of H_2 during CNT synthesis. While carbonaceous material can penetrate to the interior of the scaffold, the quality of the CNTs is compromised. At high magnification (Figure 1C Row 3), atypical CNT morphologies were observed, with ruffled CNT textures and carbonaceous impurities coating the CNTs. Due to the non-orthogonal relationships between CNT synthesis parameters,[44] it is difficult to determine the mechanism responsible for poor growth; however, such growth is indicative of a poor-quality carbon source (including suboptimal breakdown of the carbon source), as well as incorrect gas residence times and corresponding temperatures.

The optimal CNT synthesis temperature differed for the TCP/HA and Sr-HT-Gah scaffolds; CNT deposition on TCP/HA scaffolds required higher temperatures (770 ºC) than that on Sr-HT-Gah scaffolds (745 ºC). The reasons for this difference were not investigated; however interactions between CNT-growth catalysts and scaffolds are known to impact carbon breakdown over a catalyst,[44] and thus optimum synthesis parameters. Nevertheless, both ceramic scaffolds could be coated successfully, demonstrating the generality of the technique and offering promise for the coating of other thermally stable porous scaffolds with CNTs.

Analysis of CNTs Produced Under Optimized Coating Parameters

Numerous reports have emphasized the importance of using high-quality or 'pristine' CNTs in biological applications. This

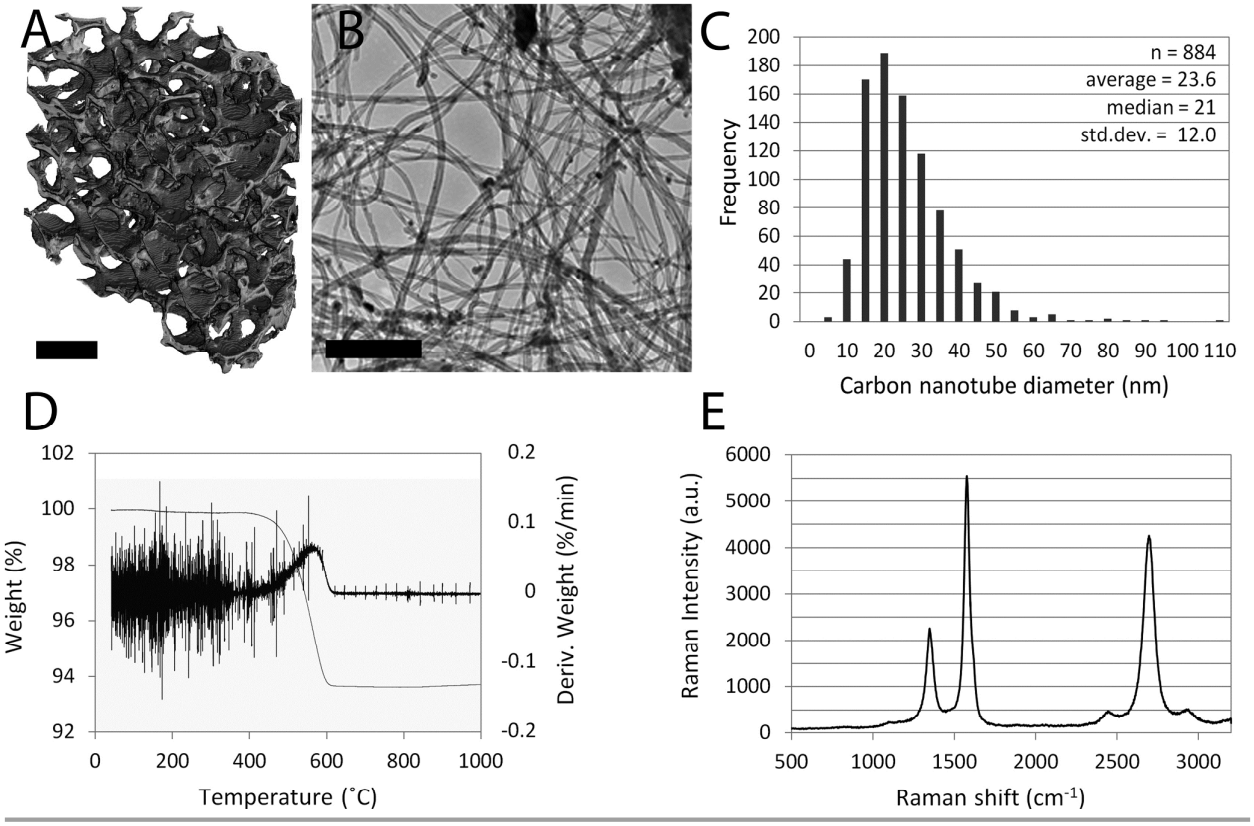

Figure 2. Dimensional, chemical and structural characteristics of the CNTs synthesized over the Sr-HT-Gah or TCP/HA scaffolds. Figure 2A shows a representative reconstruction of micro-CT data taken of a TCP/HA scaffold. The sponge-like architecture of the material resembles that of cancellous bone (scale bar = 1 mm). Figure 2B shows a representative TEM micrograph of CNTs removed from the surface of a Sr-HT-Gah scaffold (see Experimental Section for details, scale bar = 500 nm). **Error! Reference source not found.**2C is a meta-analysis of TEM micrographs showing a histogram of the diameters of CNTs removed from the surface of a Sr-HT-Gah scaffold. **Error! Reference source not found.**2D shows a characteristic thermogravimetric analysis of the CNT-coated Sr-HT-Gah scaffolds. The left axis and corresponding curve showing a total weight loss of 6 wt% from 100% to 94% with most significant weight loss (between 450 and 600 ˚C) attributable to the oxidation of CNTs in air. The right axis shows the derivative of the weight% with respect to temperature; with a peak at approximately 580 ˚C. This peak corresponds to the temperature with the highest mass loss given a change in temperature. The noise in the axis is attributable to the relatively small sample size and high sensitivity of the instrument. **Error! Reference source not found.**2E shows a characteristic Raman spectrum of CNT-coated Sr-HT-Gah scaffolds with sharp peaks characteristic of multiwalled CNTs at ~1350 cm–1 (D band), ~1580 cm–1 (G band), and ~2700 cm–1 (G' band).

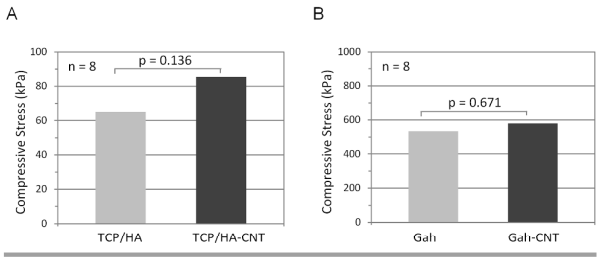

Figure 3. Comparison of the compressive strength of uncoated and CNT-coated TCP/HA and Sr-HT-Gah scaffolds, showing no significant differences upon coating (n = 8).

requires low levels of bioavailable metal from the CNT-growth catalyst precursors and high graphitic purity of the CNTs, as problems with the CNT-growth catalyst or CNT purity will significantly affect biological response, as will defects, doping or functionalization.[45,46] The quality (level of defects, purity and graphitic structure) of the CNTs synthesized here was investigated by measuring their morphological and chemical characteristics (**Error! Reference source not found.**). **Error! Reference source not found.**B shows a representative TEM micrograph revealing characteristic multiwalled-CNT morphology, including high aspect ratios and tubular structure. A morphemetric analysis of these images was conducted to determine the diameters of 884 CNTs. This data is shown as a histogram in **Error! Reference source not found.**C with average diameter of 23.6 nm over a range of 3.9–108.6 nm. This distribution was comparable to the dimensionality and range seen for collagen fibrils, the main constituent of the extracellular environment. Connective-tissue collagen fibers have been observed with average diameters between 60-80 nm and ranges between 20-140 nm.[47,48] Use of nanotopographies and fibrous structures with such dimensionality has demonstrated an ability to control stem cell fate for osteogenesis.[49,50]

Error! Reference source not found.D shows a thermogravimetric analysis characteristic of the CNT-coated Sr-HT-Gah scaffolds. Slight decreases in mass (0.1–0.2%) were observed upon heating in air from room temperature to 450 ˚C, after which there was an average decrease in sample weight of 4.38% (of total sample weight). This second decrease is attributed to the oxidation of CNTs, and the minimal changes in weight prior to this temperature indicate the high quality of the CNTs and absence of other carbon materials. **Error! Reference source not found.**E shows a Raman spectrum characteristic of CNT-coated Sr-HT-Gah scaffolds. All samples showed sharp peaks characteristic of multiwalled CNTs at ~1350 cm^{-1} (D band), ~1580 cm^{-1} (G band) and at ~2700 cm^{-1} (G' band). The relative heights of the graphitic-structure-derived G-band and the defect-derived D-band, or I_G/I_D ratio, of ~2.5 indicated a high crystal purity and low defect concentration of the CNTs.

The high quality of the CNTs is attributable to relatively high concentrations of H_2 (compared to typical synthesis conditions)[44] and the addition of the amorphous-carbon etchant CO_2[43] applied during CNT synthesis. At the low concentration used here (4500 ppm), CO_2 etches away the less-stable undesirable carbons without damaging the CNTs. Whereas dilute etchants such as CO_2 and H_2O have been known to improve CNT growth and quality,[43,51] the effects of H_2 on these characteristics have only recently been extensively quantified.[52] High H_2 concentrations are believed to play roles in cleaning and gasifying reagents during CNT synthesis, thus helping to maintain catalyst stability and increase CNT yield and quality.

Physical Properties of the Scaffolds

The physical properties of the CNT-coated scaffolds were evaluated to determine how coating impacted their surface area, porosity and mechanical properties.

Error! Reference source not found.**3** shows that there were no significant changes to the compressive strength of the TCP/HA or the Sr-HT-Gah scaffolds upon coating. Importantly, heat treatment, the CNTs themselves or procedures otherwise required to coat the scaffolds did not compromise their mechanical performance. Further, while the nominal values of compressive strength could be considered insufficient for load bearing applications, their performance given the relatively high porosities (~90%) should be stressed. Previous reports with Sr-HT-Gah scaffolds have shown that decreasing the porosity of a Sr-HT-Gah scaffold significantly increases its strength. Decreasing porosity to 80% has previously produced increases in the scaffold's compressive strength to 4.1 MPa (an approximate 8-fold increase given their strength reported herein); a strength comparable to cancellous bone.[35]

Analysis with microcomputed X-ray tomography (µCT; SkyScan 1072, Belgium) demonstrated scaffold porosities of 90.1% for Sr-HT-Gah and 92.6% for TCP/HA scaffolds. Scaffold pores had diameters in the range 580-850 µm with an interconnectivity of 100%. Porosity >80% with pores of diameters ≥300 µm is ideal for promoting tissue regrowth, as it allows cellular infiltration, the transport of nutrients/waste and bone ingrowth.[53] A cross-sectioned volume generated from CT scans of a TCP/HA scaffold is shown in Figure 2A. The porous, sponge-like structure of the scaffolds resembled the architecture of cancellous bone.

The surface area of the TCP/HA scaffolds following coating was compared using N_2 physisorption. Coated scaffolds showed a 1.36-fold increase in the Brunauer–Emmett–Teller surface area compared to the bare scaffold (3.88 and 2.85 m^2/g for coated and uncoated samples, respectively). High surfaces areas better mimic the surface-area-to-volume ratios seen in the nanofibrous structures of the extracellular matrix. Further, large surface areas potentiate further increases to scaffold bioactivity by adsorption or covalent attachment of biochemicals.[54]

Biocompatibility of the Scaffolds

Having obtained 3D porous scaffolds bearing uniform coatings of high-quality CNTs, we tested their biocompatibility through observation and measurement of cell attachment and proliferation. Comparison between the clinically used bioceramic TCP/HA and CNT-coated TCP/HA scaffolds

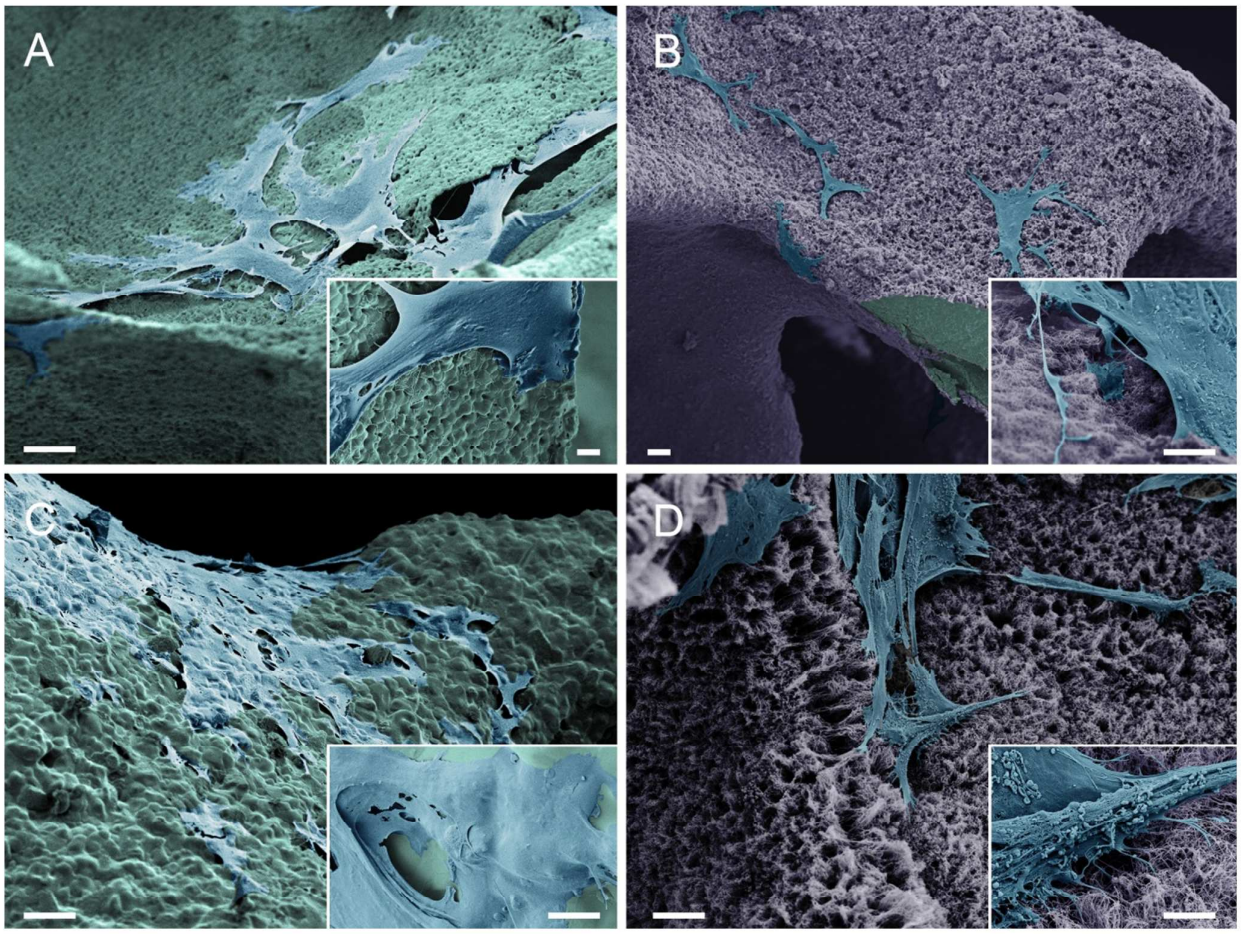

Figure 4. Scanning electron micrographs with false-colouring showing cell adhesion 24 h after seeding over A) TCP/HA B) CNT-coated TCP/HA C) Sr-HT-Gah D) CNT-coated Sr-HT-Gah. Scaffolds were fixed and cross-sectioned after cell culture. CNTs, cells and ceramics are coloured purple, dark blue, and light blue, respectively. Scale bars are 20 µm (2 µm in insets).

demonstrated biocompatibility with comparable cell attachment and equivalent proliferation.

Cell Attachment to Scaffolds

Cell attachment was shown over coated and uncoated TCP/HA and Sr-HT-Gah scaffolds using SEM analysis. ASCs were cultured for 24 h and then fixed for SEM analysis as previously described.[35,36] **Error! Reference source not found.** shows false-colored SEM images of ASC attachment to uncoated and CNT-coated scaffolds of both TCP/HA and Sr-HT-Gah (additional images are available in the Supplementary Information, Figure S1). Biocompatibility was comparable between scaffolds with cells interacting favorably with all scaffold types, showing a high degree of spreading and elongated morphologies (Figure 4). Insets in **Error! Reference source not found.**4 show high-magnification images of cells grown on the different scaffolds. Over CNT-coated scaffolds (**Error! Reference source not found.** B and D), there were more filopodia-type protrusions extending from the leading edge of the lamellipodia and interacting with the scaffolds. The large number of filopodia suggests a strong anchorage to the scaffold through filopodia-coupled adhesions. Similar observations have been made for other CNT-containing scaffolds, with reports of high numbers of attachment sites and increases to cell spreading.[19,20,23,55]

Cell Proliferation over Scaffolds

To address dissenting reports resulting from interactions of CNTs with various assays, including Commassie Blue, Alamar Blue, Neutral Red, MTT and WST assays, cell proliferation was measured using a two-step method[8,56,57] that was developed to eliminate confounding chemical interactions occur between the CNTs and the fluorescent dyes.[58] The scaffolds were therefore washed with a lysis buffer, and the cell lysates were removed from the scaffolds prior to incubation with a DNA-binding fluorescent dye. The proliferative capacity of the scaffolds was assessed for both ASCs and HOBs cell types over TCP/HA and CNT-coated TCP/HA (CNT-TCP/HA) scaffolds **Error! Reference source not found.**. Both scaffold types supported cell proliferation of ASCs over a seven-day period. There were no significant differences in proliferation on the TCP/HA and CNT-TCP/HA groups at any time point, suggesting that the biocompatibility of the CNT-coated scaffolds was comparable

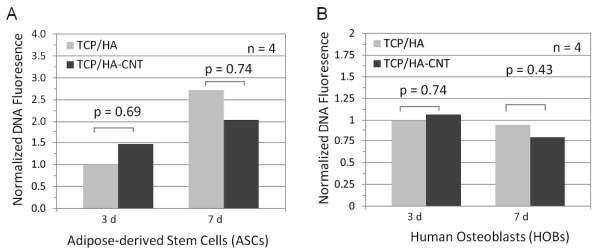

Figure 5. Relative cell proliferation determined by measuring DNA-binding protein fluorescence intensity of cells that had been separated from the scaffolds; see Experimental Section for details. Both ACSs and HOBs cells are measured at 3 and 7 d. For each cell types, proliferation is normalized to that measured on uncoated TCP/HA scaffolds at 3 d.

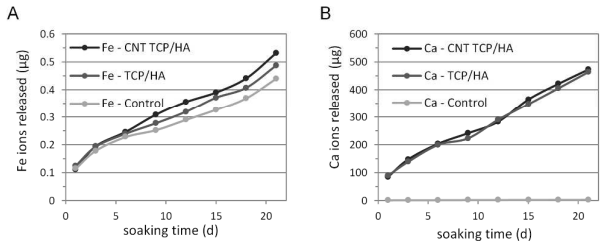

Figure 6. Leaching of Fe and Ca from scaffolds was measured using inductively coupled plasma–atomic emission spectrometry.

to the current clinical standard in ceramic bone scaffolds. For both cell types, higher DNA fluorescence intensity was observed over the CNT-coated scaffolds at day three, but relatively lower intensities were seen at day seven. Previous studies have suggested that such reduction in the proliferation of cells over CNT scaffolds is due to a slowing of the cell cycle rather than to cell death.[59]

This proliferation behavior is similar to that previously reported, with no significant differences in proliferation of osteoblasts seen between alumina and a CNT-alumina composites.[11] Further, when this alumina–CNT composite was implanted in an in vivo model, no inflammatory reaction was observed. In another in vivo study that used a non-ceramic poly(propylene fumarate)–CNT composite, a 300% increase in bone area formation was observed, compared to a control without CNTs. Further, histological scoring indicated better tissue organization, greater ingrowth and a reduced number of surrounding inflammatory cells on the CNT composite scaffold, compared to the uncoated polypropylene fumarate.[32]

The literature contains numerous dissenting reports regarding the biocompatibility of CNTs.[60] These inconsistencies reflect the variability among CNTs, including differences in functional groups or defects in their walls, in electronic nature (conducting or semiconducting), in morphology (short, long, thick, thin) and wall number, and in the presence of residual transition metals derived from the CNT-growth catalyst. Consequently, there is controversy over the mechanism by which CNTs can exhibit toxicity. It is recognized that toxic reactive oxidative species (ROS) can be created through the interactions of compounds with CNT defects, undesirable functionalisations and interaction with metal catalyst particles.[8,61] Consequently, high-purity and defect-free CNTs, such as those synthesized here (**Error! Reference source not found.**), minimize ROS formation and thus toxic potential.

Toxicity of Ions Leached from Scaffolds

CNTs are grown over metallic catalyst particles that induce the decomposition of the carbon precursor and mediate the formation of the nanotube; however, these particles have been suggested as sources of CNT toxicity.[46,62] To investigate any potential leaching of metal particles from the scaffolds, we measured Fe release from scaffolds soaked in a phosphate-buffered saline solution using inductively coupled plasma–atomic emission spectrometry (ICP–OES, Vista AX, Varian **Error! Reference source not found.**). The concentration of Fe was compared to a control solution in which no scaffolds were soaked; refer to Experimental Section for details. When compared to a control solution without scaffolds, the solutions containing CNT-coated TCP/HA scaffolds had significantly more ($p < 0.05$) Fe in solution after 9 and 12 days, whereas uncoated TCP/HA scaffolds had significantly more at 15 and 21 days. Although the Fe release was delayed over the uncoated scaffolds, the differences in amount of Fe released were not significant between CNT-coated and uncoated TCP/HA scaffolds, demonstrating that there was no significant increase in Fe release resulting from the presence of CNT-growth catalyst. Over the course of 21 days, the cumulative release of Fe from the scaffolds was <0.53 µg (0.27 ppm) (see **Error! Reference source not found.**A). This is many times smaller than the average daily absorption of iron in humans, which is approximately 1 mg,[63] vitiating concerns of Fe toxicity. Furthermore, 10–200 ppm solutions of Fe nanoparticles are routinely used for biological applications and little to no toxicological effects on human fibroblasts are observed even for concentrations of 200 ppm or greater.[64]

Importantly, CNT coating perturbed neither the degradation of, nor the release of Ca from, the TCP/HA scaffolds (**Error! Reference source not found.**6B). Accessibility and release of calcium is important as, together with phosphate, it is the main component of bone matrix. The release of Ca from such synthetic materials improves both calcification of bone extracellular matrix and bone strength. Further, Ca plays important roles in osteogenic cell signaling, including encouraging mesenchymal precursors and upregulating osteogenic differentiation.[65] Such release of bioactive molecules improves osteogenesis and thus scaffold fixation and the interfacing between newly formed bone and the synthetic scaffold.[65,66]

Discussion

Presently, the majority of studies investigating CNT toxicity in vivo demonstrate efficacy through minimal toxicity.[67] Typical studies focus on the pharmacological application and profile of CNTs including their breakdown, accumulation and clearance from biological systems. One study demonstrated no evidence of toxicity and thus efficacious use in such applications up to 4 months following treatment.[68]

In the case of bone, in vivo studies with CNTs have evinced benign integration of CNTs into the newly formed bone matrix.

[32,69] In the case of Usui et al. this was demonstrated up to 12 weeks from implantation.[10] While this demonstrates promising results, the long-term profile of CNTs in such situations is unknown and consequently future studies will have to address longer-term health outcomes including the stability of CNTs under this environment. Relevant to this study is the fact that CNT toxicity can occur when CNTs are dispersed in solution or released from a scaffold/composite, and thus are free to lyse cells, damage cell membranes, and accumulate in undesirable locations within cells. CNTs have been shown to accumulate in cellular cytoplasm[70] and organelles.[71,57] Such concerns have been raised in previous work where CNTs have induced asbestos-like pathogenicity when introduced into the mesothelial lining of mice,[72] have accumulated in the subpleural tissue of mice following inhalation,[73] or have accumulated in kidneys and lymphatic system of mice.[67]. Therefore, studies should include assessing the risk of in vivo CNT migration and bioaccumulation in undesirable locations.

Furthermore, given the established potential of CNTs for tissue engineering across a range of tissue types including bone,[10-12] cartilage,[13] muscle,[14,15] and nerve tissue,[16-18] future testing should also determine the potential application of these scaffolds with a wider range of tissue/cell types, in particular those that benefit from conductive or electrically active substrates[18]. Additionally, the bioactivity of these scaffolds could be specified through alteration to the dimensional and/or biochemical properties of the scaffolds. Dimensionality of the CNT coating can be altered by changes to synthesis parameters including carbon supply[74] or temperature,[75] and can regulate cell behavior.[1,2,76] The potential for positive contributions imparted by the nanoscale dimensionality of the CNT interface is an area of further interest. Nanodimensional alteration to a material's surface can regulate stem cell fate through changes to cell adhesion as well as morphology. These behaviors can be exploited to improve a biomaterial's regenerative capacity by directing stem cell lineage.[50,77] In such applications nanoscale features with high aspect ratios (such as CNTs) demonstrate significant upregulation of osteogenic function.[78] Such studies have demonstrated that cellular mechanisms exist in which osteogenesis is promoted through increases to cell stress. [50,79] Similar results have been replicated with the use of CNTs to create specified nanotopographies. These have shown the ability to direct stem cell behaviors towards neurogenic,[80] myogenic[15] and osteogenic lineage.[26] Given these findings the potential for the CNT-coated substrates to assist in the regulation is an area of further interest.

Alternatively the nanotubes can be chemically altered using established techniques to functionalize[19] or conjugate the scaffolds with biochemicals.[81] Such techniques have the potential to greatly increase the materials bioactivity with the delivery of tissue specific therapeutics (including growth factors, cytokines or DNA transfections).

Conclusion

We developed novel three-dimensional CNT-coated scaffolds for tissue-engineering applications. The scaffolds addressed the deficiencies of previous CNT materials for tissue engineering[10-12,19-33] by combining high porosity (90%), which allows waste/nutrient exchange and cellular ingrowth, with biocompatibility and the potential for load-bearing applications.[35] The uniform, high-quality coating of CNTs was synthesized over porous ceramic scaffolds by modifying a traditional CNT synthesis by CVD. This involved using relatively low gas-flow rates, and low concentrations of CO_2 and high concentration of H_2 in the CNT-growth phase. No further functionalization or purification steps were necessary to yield highly spread attachment of ASCs and proliferation of both ASCs and HOBs comparable to that observed on the TCP/HA clinical standard for synthetic ceramic scaffolds. Low levels of bioavailable Fe were found, removing concerns about potential toxicity from the metallic CNT-growth-catalyst particles.

Acknowledgements

The authors gratefully acknowledge the financial support of the Commonwealth Government for providing an Australian Postgraduate Award Scholarship to P.N. The Australian National Health and Medical Research Council, the Rebecca Copper Foundation and the Australian Research Council are also acknowledged for financial support. The authors acknowledge the facilities of the Australian Microscopy and Microanalysis Research Facility at the Australian Centre for Microscopy and Microanalysis, The University of Sydney, and the scientific and technical assistance with SEM, TEM and CT analysis that was provided by Mr. Victor Lo and Dr. Matthew Foley.

Notes and References

1. C. J. Bettinger, R. Langer and J. T. Borenstein, *Angew Chem Int Edit*, 2009, **48**, 5406-5415.
2. T. Dvir, B. P. Timko, D. S. Kohane and R. Langer, *Nature nanotechnology*, 2011, **6**, 13-22.
3. J. N. Coleman, U. Khan, W. J. Blau and Y. K. Gun'ko, *Carbon*, 2006, **44**, 1624-1652.
4. .M. Zhang, S. L. Fang, A. A. Zakhidov, S. B. Lee, A. E. Aliev, C. D. Williams, K. R. Atkinson and R. H. Baughman, *Science*, 2005, **309**, 1215-1219.
5. O. Breuer and U. Sundararaj, *Polym Composite*, 2004, **25**, 630-645.
6. C. Li, E. T. Thostenson and T. W. Chou, *Compos Sci Technol*, 2008, **68**, 1227-1249.
7. M. Endo, M. S. Strano and P. M. Ajayan, *Top Appl Phys*, 2008, **111**, 13-61.
8. P. Newman, A. Minett, R. Ellis-Behnke and H. Zreiqat, *Nanomed-Nanotechnol*, 2013, **9**, 1139-1158.
9. N. Saito, H. Haniu, Y. Usui, K. Aoki, K. Hara, S. Takanashi, M. Shimizu, N. Narita, M. Okamoto, S. Kobayashi, H. Nomura, H. Kato, N. Nishimura, S. Taruta and M. Endo, *Chem Rev*, 2014, **114**, 6040-6079.
10. Y. Usui, K. Aoki, N. Narita, N. Murakami, I. Nakamura, K. Nakamura, N. Ishigaki, H. Yamazaki, H. Horiuchi, H. Kato, S. Taruta, Y. A. Kim, M. Endo and N. Saito, *Small*, 2008, **4**, 240-246.

11. N. Ogihara, Y. Usui, K. Aoki, M. Shimizu, N. Narita, K. Hara, K. Nakamura, N. Ishigaki, S. Takanashi, M. Okamoto, H. Kato, H. Haniu, N. Ogiwara, N. Nakayama, S. Taruta and N. Saito, *Nanomedicine-Uk*, 2012, **7**, 981-993.
12. M. Shimizu, Y. Kobayashi, T. Mizoguchi, H. Nakamura, I. Kawahara, N. Narita, Y. Usui, K. Aoki, K. Hara, H. Haniu, N. Ogihara, N. Ishigaki, K. Nakamura, H. Kato, M. Kawakubo, Y. Dohi, S. Taruta, Y. A. Kim, M. Endo, H. Ozawa, N. Udagawa, N. Takahashi and N. Saito, *Adv Mater*, 2012, **24**, 2176-2185.
13. N. O. Chahine, N. M. Collette, C. B. Thomas, D. C. Genetos and G. G. Loots, *Tissue Eng Pt A*, 2014, **20**, 2305-2315.
14. R. A. MacDonald, B. F. Laurenzi, G. Viswanathan, P. M. Ajayan and J. P. Stegemann, *J Biomed Mater Res A*, 2005, **74A**, 489-496.
15. A. F. Quigley, J. M. Razal, M. Kita, R. Jalili, A. Gelmi, A. Penington, R. Ovalle-Robles, R. H. Baughman, G. M. Clark, G. G. Wallace and R. M. I. Kapsa, *Adv Healthc Mater*, 2012, **1**, 801-808.
16. H. Hu, Y. C. Ni, V. Montana, R. C. Haddon and V. Parpura, *Nano Lett*, 2004, **4**, 507-511.
17. E. Jan and N. A. Kotov, *Nano Lett*, 2007, **7**, 1123-1128.
18. D. Y. Lewitus, J. Landers, J. R. Branch, K. L. Smith, G. Callegari, J. Kohn and A. V. Neimark, *Adv Funct Mater*, 2011, **21**, 2624-2632.
19. L. P. Zanello, B. Zhao, H. Hu and R. C. Haddon, *Nano Lett*, 2006, **6**, 562-567.
20. S. Y. Park, S. Y. Park, S. Namgung, B. Kim, J. Im, Y. Kim, K. Sun, K. B. Lee, J. M. Nam, Y. Park and S. Hong, *Adv Mater*, 2007, **19**, 2530-+.
21. K. Y. Baik, S. Y. Park, K. Heo, K. B. Lee and S. Hong, *Small*, 2011, **7**, 741-745.
22. C. Y. Tay, H. G. Gu, W. S. Leong, H. Y. Yu, H. Q. Li, B. C. Heng, H. Tantang, S. C. J. Loo, L. J. Li and L. P. Tan, *Carbon*, 2010, **48**, 1095-1104.
23. A. O. Lobo, M. A. F. Corat, E. F. Antunes, M. B. S. Palma, C. Pacheco-Soares, E. E. Garcia and E. J. Corat, *Carbon*, 2010, **48**, 245-254.
24. T. R. Nayak, L. Jian, L. C. Phua, H. K. Ho, Y. P. Ren and G. Pastorin, *Acs Nano*, 2010, **4**, 7717-7725.
25. S. Namgung, T. Kim, K. Y. Baik, M. Lee, J. M. Nam and S. Hong, *Small*, 2011, **7**, 56-61.
26. S. Namgung, K. Y. Baik, J. Park and S. Hong, *Acs Nano*, 2011, **5**, 7383-7390.
27. S. Mwenifumbo, M. S. Shaffer and M. M. Stevens, *J Mater Chem*, 2007, **17**, 1894-1902.
28. A. Abarrategi, M. C. Gutierrez, C. Moreno-Vicente, M. J. Hortiguela, V. Ramos, J. L. Lopez-Lacomba, M. L. Ferrer and F. del Monte, *Biomaterials*, 2008, **29**, 94-102.
29. E. Hirata, M. Uo, H. Takita, T. Akasaka, F. Watari and A. Yokoyama, *J Biomed Mater Res B*, 2009, **90B**, 629-634.
30. M. Bhattacharya, P. Wutticharoenmongkol-Thitiwongsawet, D. T. Hamamoto, D. Lee, T. H. Cui, H. S. Prasad and M. Ahmad, *J Biomed Mater Res A*, 2011, **96A**, 75-82.
31. F. Mei, J. S. Zhong, X. P. Yang, X. Y. Ouyang, S. Zhang, X. Y. Hu, Q. Ma, J. G. Lu, S. Ryu and X. L. Deng, *Biomacromolecules*, 2007, **8**, 3729-3735.
32. B. Sitharaman, X. F. Shi, X. F. Walboomers, H. B. Liao, V. Cuijpers, L. J. Wilson, A. G. Mikos and J. A. Jansen, *Bone*, 2008, **43**, 362-370.
33. R. Touri, F. Moztarzadeh, Z. Sadeghian, D. Bizari, M. Tahriri and M. Mozafari, *Biomed Res Int*, 2013, DOI: Artn 465086 Doi 10.1155/2013/465086.
34. A. R. Boccaccini, F. Chicatun, J. Cho, O. Bretcanu, J. A. Roether, S. Novak and Q. Chen, *Adv Funct Mater*, 2007, **17**, 2815-2822.
35. S. I. Roohani-Esfahani, C. R. Dunstan, J. J. Li, Z. Lu, B. Davies, S. Pearce, J. Field, R. Williams and H. Zreiqat, *Acta Biomater*, 2013, **9**, 7014-7024.
36. S. I. Roohani-Esfahani, Y. J. Chen, J. Shi and H. Zreiqat, *Mater Lett*, 2013, **107**, 378-381.
37. M. S. Dresselhaus, G. Dresselhaus, R. Saito and A. Jorio, *Phys Rep*, 2005, **409**, 47-99.
38. F. M. Huang, K. T. Yue, P. H. Tan, S. L. Zhang, Z. J. Shi, X. H. Zhou and Z. N. Gu, *J Appl Phys*, 1998, **84**, 4022-4024.
39. S. Brunauer, P. H. Emmett and E. Teller, *J Am Chem Soc*, 1938, **60**, 309-319.
40. E. P. Barrett, L. G. Joyner and P. P. Halenda, *J Am Chem Soc*, 1951, **73**, 373-380.
41. L. J. Jones, M. Gray, S. T. Yue, R. P. Haugland and V. L. Singer, *J Immunol Methods*, 2001, **254**, 85-98.
42. E. Roduner, *Chemical Society reviews*, 2006, **35**, 583-592.
43. X. S. Yang, L. X. Yuan, V. K. Peterson, Y. B. Yin, A. I. Minett and A. T. Harris, *J Phys Chem C*, 2011, **115**, 14093-14097.
44. K. J. MacKenzie, O. M. Dunens and A. T. Harris, *Ind Eng Chem Res*, 2010, **49**, 5323-5338.
45. G. Oberdorster, E. Oberdorster and J. Oberdorster, *Environ Health Persp*, 2005, **113**, 823-839.
46. J. P. Kaiser, H. F. Krug and P. Wick, *Nanomedicine-Uk*, 2009, **4**, 57-63.
47. K. L. Goh, J. Hiller, J. L. Haston, D. F. Holmes, K. E. Kadler, A. Murdoch, J. R. Meakin and T. J. Wess, *Bba-Gen Subjects*, 2005, **1722**, 183-188.
48. S. Habelitz, M. Balooch, S. J. Marshall, G. Balooch and G. W. Marshall, *J Struct Biol*, 2002, **138**, 227-236.
49. W. Q. Chen, Y. Shao, X. Li, G. Zhao and J. P. Fu, *Nano Today*, 2014, **9**, 759-784.
50. M. J. Dalby, N. Gadegaard and R. O. C. Oreffo, *Nat Mater*, 2014, **13**, 558-569.
51. K. Hata, D. N. Futaba, K. Mizuno, T. Namai, M. Yumura and S. Iijima, *Science*, 2004, **306**, 1362-1364.
52. K. J. MacKenzie, O. M. Dunens and A. T. Harris, *Carbon*, 2013, **59**, 344-365.
53. D. W. Hutmacher, *Biomaterials*, 2000, **21**, 2529-2543.
54. I. Lynch and K. A. Dawson, *Nano Today*, 2008, **3**, 40-47.
55. M. Kalbacova, M. Kalbac, L. Dunsch and U. Hempel, *Carbon*, 2007, **45**, 2266-2272.
56. A. Casey, E. Herzog, M. Davoren, F. M. Lyng, H. J. Byrne and G. Chambers, *Carbon*, 2007, **45**, 1425-1432.
57. J. M. Worle-Knirsch, K. Pulskamp and H. F. Krug, *Nano Lett*, 2006, **6**, 1261-1268.
58. H. Ali-Boucetta, K. T. Al-Jamal and K. Kostarelos, *Methods in molecular biology*, 2011, **726**, 299-312.
59. J. Holy, E. Perkins and X. Yu, *Iet Nanobiotechnol*, 2011, **5**, 41-46.
60. K. Kostarelos, A. Bianco and M. Prato, *Nature nanotechnology*, 2009, **4**, 627-633.
61. P. Miralles, T. L. Church and A. T. Harris, *Environ Sci Technol*, 2012, **46**, 9224-9239.
62. K. Pulskamp, S. Diabate and H. F. Krug, *Toxicol Lett*, 2007, **168**, 58-74.
63. T. H. Bothwell, *Nutr Rev*, 1995, **53**, 237-245.
64. S. J. Soenen, M. De Cuyper, S. C. De Smedt and K. Braeckmans, *Methods in enzymology*, 2012, **509**, 195-224.
65. A. Hoppe, N. S. Guldal and A. R. Boccaccini, *Biomaterials*, 2011, **32**, 2757-2774.
66. N. J. Lakhkar, I. H. Lee, H. W. Kim, V. Salih, I. B. Wall and J. C. Knowles, *Advanced drug delivery reviews*, 2013, **65**, 405-420.
67. C. P. Firme and P. R. Bandaru, *Nanomed-Nanotechnol*, 2010, **6**, 245-256.
68. M. L. Schipper, N. Nakayama-Ratchford, C. R. Davis, N. W. S. Kam, P. Chu, Z. Liu, X. M. Sun, H. J. Dai and S. S. Gambhir, *Nature nanotechnology*, 2008, **3**, 216-221.
69. E. Hirata, M. Uo, H. Takita, T. Akasaka, F. Watari and A. Yokoyama, *Carbon*, 2011, **49**, 3284-3291.
70. A. E. Porter, M. Gass, K. Muller, J. N. Skepper, P. A. Midgley and M. Welland, *Nature nanotechnology*, 2007, **2**, 713-717.

71. E. Mooney, P. Dockery, U. Greiser, M. Murphy and V. Barron, *Nano Lett*, 2008, **8**, 2137-2143.
72. C. A. Poland, R. Duffin, I. Kinloch, A. Maynard, W. A. H. Wallace, A. Seaton, V. Stone, S. Brown, W. MacNee and K. Donaldson, *Nature nanotechnology*, 2008, **3**, 423-428.
73. J. P. Ryman-Rasmussen, M. F. Cesta, A. R. Brody, J. K. Shipley-Phillips, J. I. Everitt, E. W. Tewksbury, O. R. Moss, B. A. Wong, D. E. Dodd, M. E. Andersen and J. C. Bonner, *Nature nanotechnology*, 2009, **4**, 747-751.
74. C. G. Lu and J. Liu, *J Phys Chem B*, 2006, **110**, 20254-20257.
75. C. Ducati, I. Alexandrou, M. Chhowalla, G. A. J. Amaratunga and J. Robertson, *J Appl Phys*, 2002, **92**, 3299-3303.
76. S. Oh, K. S. Brammer, Y. S. J. Li, D. Teng, A. J. Engler, S. Chien and S. Jin, *Proceedings of the National Academy of Sciences of the United States of America*, 2009, **106**, 2130-2135.
77. R. A. Marklein and J. A. Burdick, *Adv Mater*, 2010, **22**, 175-189.
78. K. A. Kilian, B. Bugarija, B. T. Lahn and M. Mrksich, *Proceedings of the National Academy of Sciences of the United States of America*, 2010, **107**, 4872-4877.
79. C. M. Kirschner and K. S. Anseth, *Small*, 2013, **9**, 578-584.
80. L. Fan, C. Feng, W. M. Zhao, L. Qian, Y. Q. Wang and Y. D. Li, *Nano Lett*, 2012, **12**, 3668-3673.
81. Z. Liu, S. M. Tabakman, Z. Chen and H. J. Dai, *Nat Protoc*, 2009, **4**, 1372-1382.